Phosphorescence

International Edition: DOI: 10.1002/anie.201601252
German Edition: DOI: 10.1002/ange.201601252

Versatile Room-Temperature-Phosphorescent Materials Prepared from N-Substituted Naphthalimides: Emission Enhancement and Chemical Conjugation

Xiaofeng Chen[+], Cheng Xu[+], Tao Wang, Cao Zhou, Jiajun Du, Zhongping Wang, Hangxun Xu, Tongqing Xie, Guoqiang Bi, Jun Jiang, Xuepeng Zhang, James N. Demas, Carl O. Trindle, Yi Luo, and Guoqing Zhang**

Abstract: *Purely organic materials with room-temperature phosphorescence (RTP) are currently under intense investigation because of their potential applications in sensing, imaging, and displaying. Inspired by certain organometallic systems, where ligand-localized phosphorescence ($^3\pi$-π^*) is mediated by ligand-to-metal or metal-to-ligand charge transfer (CT) states, we now show that donor-to-acceptor CT states from the same organic molecule can also mediate π-localized RTP. In the model system of N-substituted naphthalimides (NNIs), the relatively large energy gap between the NNI-localized $^1\pi$-π^* and $^3\pi$-π^* states of the aromatic ring can be bridged by intramolecular CT states when the NNI is chemically modified with an electron donor. These NNI-based RTP materials can be easily conjugated to both synthetic and natural macromolecules, which can be used for RTP microscopy.*

Room temperature phosphorescent (RTP) materials are useful in a plethora of important applications such as sensing, imaging, and displaying.[1–4] A key method for promoting RTP is to enhance the efficiency of intersystem crossing (ISC).[5] Generally speaking, ISC is efficient in organometallic systems,[6,7] possibly because of 1) heavy and/or paramagnetic metal ions, which can enhance spin–orbit coupling,[8] or 2) the presence of closely spaced singlet and triplet ligand-to-metal (LMCT) or metal-to-ligand charge transfer (MLCT) states (^{1}LMCT/^{3}LMCT or ^{1}MLCT/^{3}MLCT); the poor superposition of an orbital from the metal and another from the ligand results in very small singlet–triplet energy splitting (ΔE_{ST}). If the ligand-localized triplet state (^{3}IL* or $^3\pi$-π^*) happens to be the lowest in the metal complex, then ^{3}LMCT or ^{3}MLCT readily relaxes to $^3\pi$-π^* and may give rise to ligand-localized RTP under suitable conditions.[9] Alternatively, metal ions simply induce an intraligand CT state that leads to more efficient ISC, as we and others recently demonstrated that fluorescence/RTP dual emission can be achieved for many aromatic ketone/Lewis acid systems.[10,11]

Organometallic systems have some intrinsic problems, such as toxicity and instability in aqueous environments. Thus an alternative approach to achieve RTP with purely organic, water-stable compounds is highly desirable. Many purely organic RTP systems based on carbonyl or heavy-atom chemistry have been developed and have found important applications.[12–16] However, for these systems, the chemistry is very limited (i.e., carbonyl groups or halogen substituents). Herein, we report a molecular RTP system that is based on N-substituted naphthalimides (NNIs; Scheme 1), which combine many benefits, such as easy synthesis, facile chemical modification, and water stability. Although derivatives of NNIs have been frequently reported owing to their popularity in optoelectronic applications,[17,18] the observation of RTP[19,20] in this type of molecules is rare. We show here that heavy-atom induction of RTP is not necessary for NNIs when an electron donor is introduced.

As shown in Scheme 2, the inefficient RTP of NNI derivatives may be due to the large singlet–triplet energy gap (ΔE_{ST}) that is intrinsic to π–π* transitions. As previously reported, the poor overlap between the HOMO and LUMO of intramolecular charge transfer (ICT) states could result in a reduced ΔE_{ST} and thus enhanced ISC processes.[4] Therefore, ICT states introduced into molecules with dominant π–π* transitions may serve to bridge the large ΔE_{ST} and resulted in RTP under suitable conditions (e.g., in deoxygenated polymers). Compounds **1**–**4** (see the Supporting Information for their synthesis) were co-dissolved with PMMA in CH_2Cl_2 (0.5%, dye/PMMA, w/w), and the solution mixtures were then dried in glass tubes to form clear homogenous films (ca. 0.2 mm). The steady-state emission spectra of **1** and **2** in the films under air show featureless bands around 450 nm while **3** and **4** are almost non-fluorescent (Figure 1b). When the tubes were sealed under vacuum, however, the emissions of **1** and **2**

[*] X. Chen,[+] Dr. C. Xu,[+] T. Wang, C. Zhou, T. Xie, Prof. G. Bi, Prof. J. Jiang, Dr. X. Zhang, Prof. Y. Luo, Prof. G. Zhang
Hefei National Laboratory for Physical Sciences at the Microscale
University of Science and Technology of China
230026 Hefei (P.R. China)
E-mail: zhangxp@mail.ustc.edu.cn
gzhang@ustc.edu.cn
X. Chen,[+] J. Du, Prof. H. Xu
Department of Polymer Science and Engineering
University of Science and Technology of China
230026 Hefei (P.R. China)
Prof. Z. Wang
Physics Experiment Teaching Center
University of Science and Technology of China
230026 Hefei (P.R. China)
Prof. J. N. Demas, Prof. C. O. Trindle
Department of Chemistry, University of Virginia
Charlottesville, VA 22903 (USA)
[+] These authors contributed equally to this work.
Supporting information and the ORCID identification numbers for the authors of this article can be found under http://dx.doi.org/10.1002/anie.201601252.

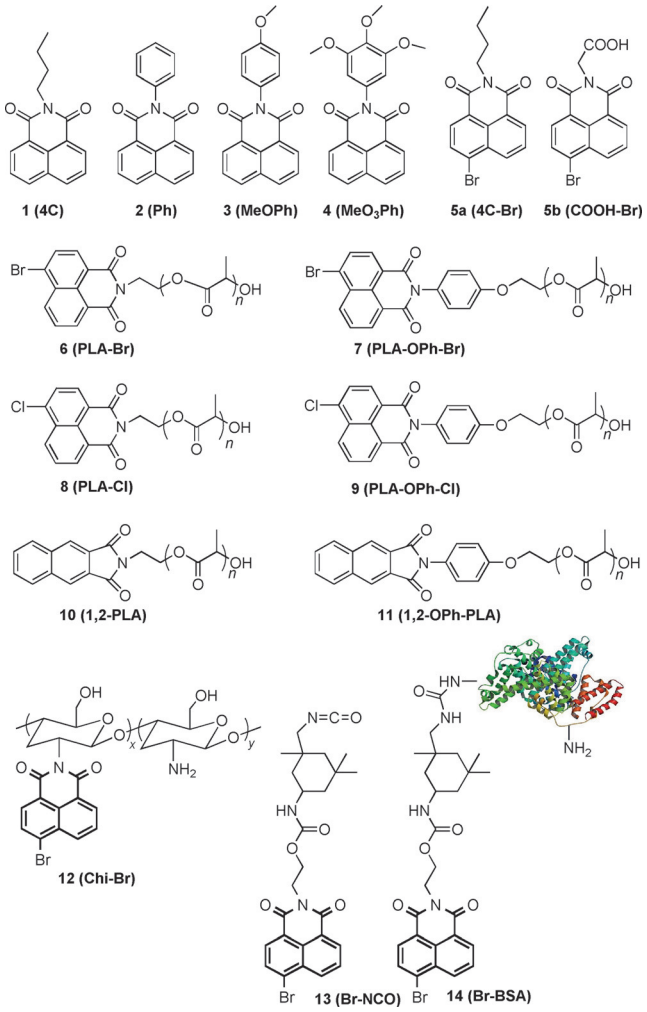

Scheme 1. Chemical structures of the naphthalimide-based organic dyes.

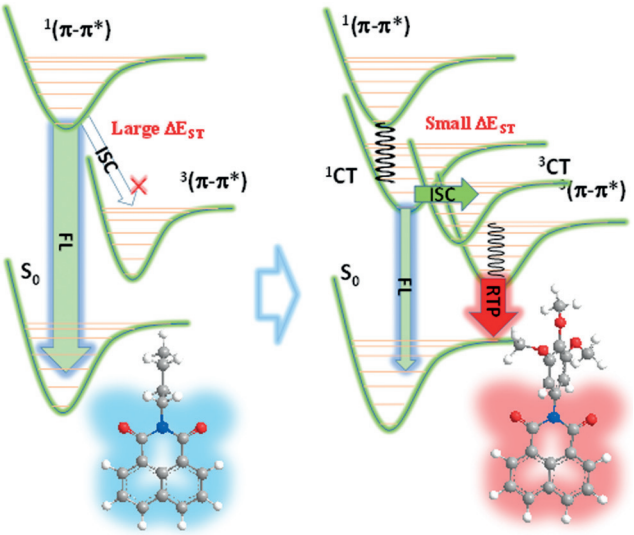

Scheme 2. Design strategy for enhancing the room-temperature phosphorescence of naphthalimide-based organic dyes.

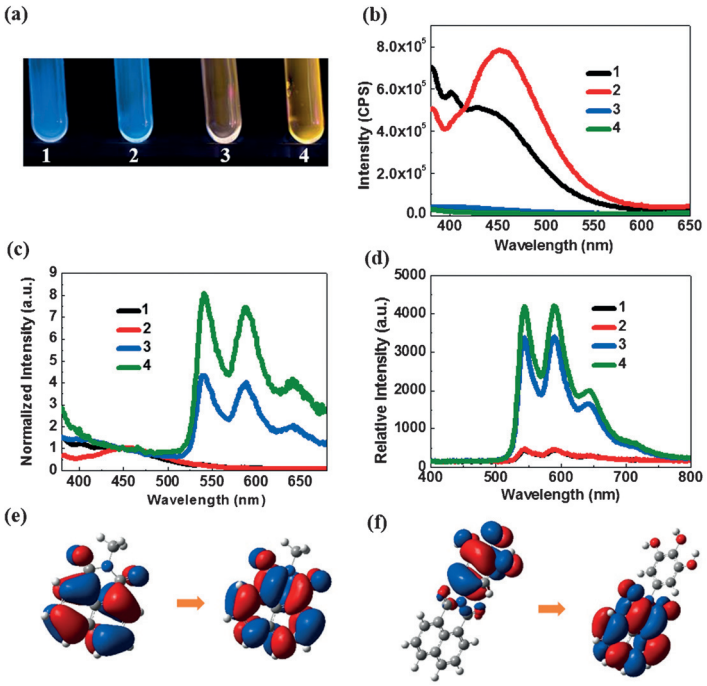

Figure 1. a) Photographs of **1**–**4** in PMMA films in vacuo under 365 nm UV excitation. b,c) Steady-state emission spectra of **1**–**4** in PMMA under air (b) and in vacuo (c). d) Delayed emission spectra of **1**–**4** in PMMA in vacuo ($\Delta t = 100$ ms, $\lambda_{ex} = 365$ nm). e,f) Calculated lowest singlet transitions for simplified **1** (e) and **4** (f).

exhibited little visual alterations but strong yellow emissions from **3** and **4** were "turned on". As shown in Figure 1c, the steady-state emission spectra of **1** and **2** in PMMA films under vacuum do not show dramatic changes compared to those in air, whereas two emission peaks centered at $\lambda = 541$ nm and 588 nm emerged for both **3** and **4** in vacuo. The blue luminescence centered at $\lambda_{em} = 450$ nm has a lifetime of 16.7 ns (Table 1, $\Phi = 0.046$) and 19.7 ns ($\Phi = 0.032$) for **1** and **2**, respectively. In contrast, the lifetime of the fluorescence of **3** and **4** at $\lambda_{em} = 541$ nm was measured to be approximately 0.23 s ($\Phi = 0.031$ and 0.039). All lifetimes can be fit to a triple-exponential decay presumably owing to the heterogeneous nature of the polymer matrix and possible dye–dye interactions. The emissions with ultralong lifetimes were convinc-

Table 1: Lifetimes and quantum yields of **1**–**5a** in PMMA under vacuum.

	1	2	3	4	5a
τ_F[a]	16.7 ns (450 nm)	19.7 ns (450 nm)	–[b]	–[b]	4.2 ns (425 nm)
τ_{RTP}[a]	–[b]	–[b]	0.23 s (541 nm)	0.23 s (541 nm)	5.1 ms (611 nm)
Φ[c]	0.046	0.032	0.0011	< 0.001	0.013
Φ[d]	< 0.001	0.0013	0.031	0.039	0.050

[a] Excitation source: 369 nm light-emitting diode; lifetime fit to triple-exponential decay (see the Supporting Information). [b] Emission too weak for reliable lifetime measurements. [c] Absolute photoluminescence quantum yield from 400–500 nm. [d] Absolute photoluminescence quantum yield from 500–750 nm.

ingly ascribed to room-temperature phosphorescence (RTP). The RTP spectra for all four molecules (Figure 1 d) are almost identical and show vibration progressions of the aromatic ring, that is, the emission peaks at 541 nm, 588 nm, and 642 nm are separated by approximately 1500 cm^{-1}, which indicates that the lowest excited triplet states are π-localized excited states $^3\pi$-π* for all molecules. This is also consistent with the observed sub-second lifetimes. All four molecules share the same electron-deficient, π-conjugated NNI ring. However, the N substituents exhibit increasing electron-donating capability, and thus the ΔE_{ST} values of the ICT states in the four compounds are expected to be in the order $\Delta E_{ST}(\mathbf{4}) < \Delta E_{ST}(\mathbf{3}) < \Delta E_{ST}(\mathbf{2}) < \Delta E_{ST}(\mathbf{1})$. To confirm this hypothesis, using the S1-optimized geometry computed with ωB97XD/cc-pVDZ[21] and the Tomasi model for the CH_2Cl_2 solvent,[22] we conducted TDDFT calculations in GAMESS.[23,24] The lambda statistic (Λ) employed by Peach et al.,[25] which measures the locality extent excitations, enables the determination of their CT character. The lambda value can range from 0 to 1, where the limits indicate disjoint (Λ→0) and common (Λ→1) spaces occupied by the origin and destination states of an excitation. The calculations show that the fluorescence is an emission from an allowed state at about 3.3 eV for each *N*-aryl species (see the Supporting Information, Table S1). These are well-localized excitations with $\Lambda > 0.8$ in each case. Orbital representations confirm that these transitions are local to the NI frame (Figure 1 e). The lowest singlet transitions from **3** and **4** are unambiguously CT states (Figure 1 f, $\Lambda = 0.099$ and 0.083) with a forbidden nature (dark state). This explains the lack of fluorescence for **3** and **4** even in the solid-state films.

It is well-known that heavy atoms can help populate triplet excitons by spin–orbit coupling. As shown in Figure 2 a, the steady-state emission spectra of compound **5a** in PMMA film (0.5 % by weight) in air exhibit two major bands with their maxima at $\lambda_F = 420$ nm (4.2 ns) and $\lambda_{RTP} = 611$ nm (5.1 ms). Compared to the ultralong "afterglow" of **3** and **4** ($\tau_{RTP} \approx 0.23$ s), the RTP of **5a** has a much shorter lifetime and could not be entirely quenched even when exposed to air (see Figure 2 a, b). This is likely due to the enhanced triplet to (singlet) ground state decay rate from the heavy atom effect, which outcompetes the relatively slow oxygen diffusion in PMMA film (ca. 0.2 mm). When a hydrophilic group is used to replace the butyl group (**5b**), RTP could also be detected in deoxygenated buffer solution (Figure 2 c, d) but with a shorter lifetime (0.5 ms) and lower relative intensity, which is presumably due to activated collisional quenching.

The experimental luminescence results for **5a** and **5b** are consistent with a recent report by Taddei and co-workers,[20] where RTP in both organic solution and the crystalline state was observed for a Br-substituted NNI derivative. However, we show in the following experiments that the RTP/fluorescence ratio can be further increased by the ICT enhancement strategy (**6**–**11**). Introducing a heavy halogen atom (**6**–**9**) or extending the π-conjugation (**10** and **11**) can affect the miscibility between the NNI dye and the polymer matrix; we thus resorted to the method of covalent dye conjugation with a polymer by ring-opening polymerization (ROP), which was developed by Fraser and co-workers.[26] To extend the potential of NNI-based phosphorescent molecules in biological imaging, we also synthesized a series of NNI-based ROP initiators **I1**–**I6** (Scheme S1), from which the luminescent PLAs **6**–**11** (Scheme 1) were made. NMR spectra and gel permeation chromatography (GPC) data (see the Supporting Information) indicate that polymers **6**–**11** are well-defined (PDI < 1.15), and their molecular weights are given in Table 2.

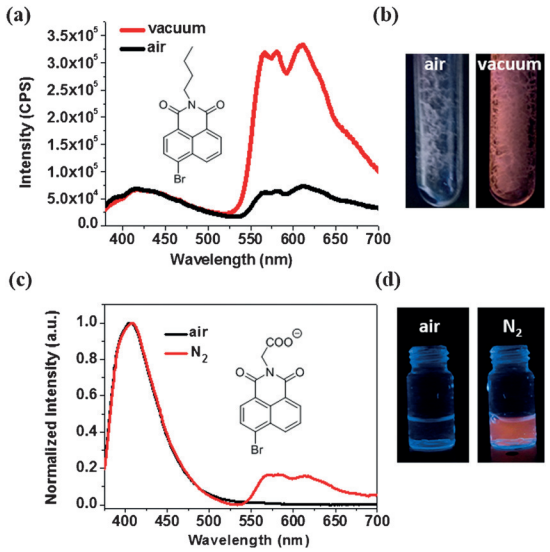

Figure 2. a) Steady-state emission spectra of **5a** in PMMA under air (black) and in vacuo (red). b) Photographs of **5a** in PMMA film under air and in vacuo ($\lambda_{ex} = 365$ nm). c) Steady-state emission spectra of **5b** in a pH 6.8 buffer before (black) and after deoxygenation (red). d) Photographs of **5b** buffer solutions in air and after purging with nitrogen gas ($\lambda_{ex} = 365$ nm).

Table 2: Molecular weight data of polymers **6**–**11**.

	6	**7**	**8**	**9**	**10**	**11**
M_n (NMR)[a]	5200	4900	7000	6500	10000	11000
M_n (GPC)[b]	11000	9300	10400	17400	14500	12800
PDI (GPC)[c]	1.09	1.06	1.04	1.14	1.11	1.10

[a] Number-average molecular weight calculated from the integration ratio of the CH (PLA) proton and residual initiator protons in NMR spectra recorded in $CDCl_3$. [b] Number-average molecular weight determined by GPC using THF as the eluent at 25 °C; the system was calibrated with linear polystyrene standards. A correction factor of 0.58 for PLA was applied to all data.[26] [c] Polydispersity index (PDI = M_w/M_n).

As shown in Figure 3 a, films of **6** (PLA-Br), **7** (PLA-OPh-Br), **9** (PLA-OPh-Cl), and **11** (1,2-OPh-PLA) exhibit barely detectable steady-state emission under 365 nm excitation in air, whereas emissions centered at 412 nm and 385 nm were observed for **8** (PLA-Cl) and **10** (1,2-PLA), respectively. After sealing the PLA films under vacuum, a dramatic increase in the emission intensity of the lower-energy band (500–700 nm) was observed for all polymers except for **10**, whose emission hardly changed. The luminescence lifetimes of the newly added emissions for **6**, **7**, **8**, **9**, and **11** were measured to be $\tau = 5.6$ ms ($\lambda_{em} = 611$ nm), 3.6 ms ($\lambda_{em} =$

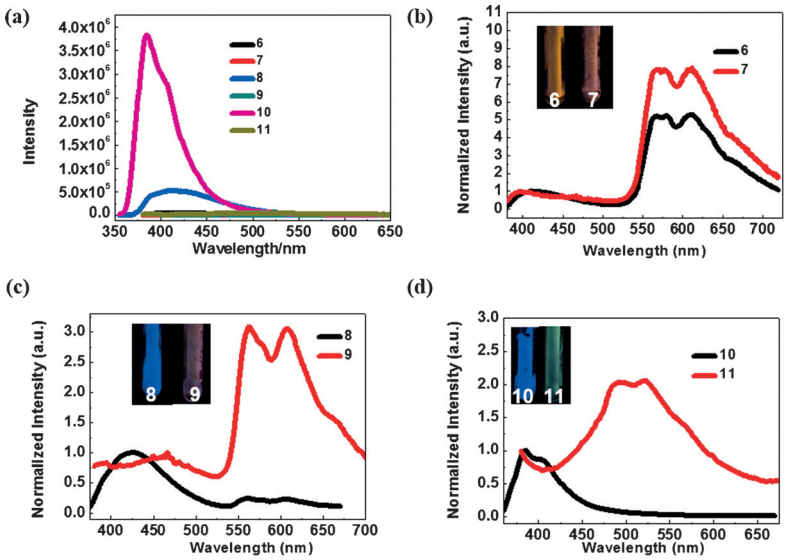

Figure 3. a) Steady-state emission spectra of **6**–**11** in air. b) Steady-state emission spectra of **6** and **7** in vacuo normalized to the fluorescence band. Inset: Corresponding photographs of **6** and **7**. c) Steady-state emission spectra of **8** and **9** in vacuo normalized to the fluorescence band. Inset: Corresponding photographs of **8** and **9**. d) Steady-state emission spectra of **10** and **11** in vacuo normalized to the fluorescence band. Inset: Corresponding photographs of **10** and **11** ($\lambda_{ex}=365$ nm).

611 nm), 84 ms ($\lambda_{em}=607$ nm), 70 ms ($\lambda_{em}=607$ nm), and 1.12 s ($\lambda_{em}=510$ nm), respectively (Table 3). These millisecond to second lifetimes are characteristic of RTP of $^3\pi$-π^* origin. The lifetimes of the shorter-wavelength emissions for **6**, **8**, **9**, and **10** were measured to be $\tau=1.75$ ns ($\lambda_{em}=413$ nm), 7.0 ns ($\lambda_{em}=425$ nm), 7.1 ns ($\lambda_{em}=450$ nm), and 7.3 ns ($\lambda_{em}=385$ nm), respectively, which are ascribed to fluorescence.

The presence of either a heavy atom (Cl or Br) or ICT provides **6**, **7**, **8**, **9**, and **11** with sufficient ISC efficiency to allow for strong RTP. Compared to Cl, the heavier Br should have a more significant heavy-atom effect on the NNI derivatives by stronger spin–orbit coupling. Therefore, considering the comparable photoluminescence quantum yields (ca. 0.03–0.06 in PLA; Table 3), **6** has a larger RTP/fluorescence intensity ratio (I_{RTP}/I_{FL}) as well as a shorter RTP lifetime than **8**. Similarly, the I_{RTP}/I_{FL} ratio of **7** is larger than that of **9**, and the RTP lifetime of **7** is also about 10 times shorter than that of **9**. On the other hand, **7** and **9** benefit from ISC enhancement by both heavy-atom effects and ICT, whereas **6** and **8** only take advantage of heavy-atom effects; thus the observed RTP of **7** (or **9**) is more prominent than that of **6** (or **8**), as indicated by the normalized steady-state emission spectra (Figure 3b,c). Compared to polymers **6**–**9**, the RTP of **11**, which was synthesized to show the most dramatic CT effect given its large ΔE_{ST} (ca. 56 kcal mol^{-1}) and thus inefficient ISC, is enhanced only by ICT. This exerts a substantial effect in increasing the rate of ISC ($S^*\rightarrow T_1$) but plays a minor role (e.g., vibrational coupling) on the transition from $^3\pi$-π^* to the ground state ($T_1\rightarrow S_0$). As a result, the lifetime of the phosphorescence of **11** is as long as 1.12 s, one of the longest RTP lifetimes for purely organic molecules ever reported.

Aside from the synthetic polymers, we also conducted facile modifications to these NNI-based dyes with natural biomacromolecules, using chitosan and bovine serum albumin (BSA) as two examples. Visually, NNI-modified chitosan **12** showed red RTP when illuminated with 365 nm UV light at room temperature even in air. As shown in Figure 4a, the emission spectra of **12** exhibit an RTP band around 600 nm (5.3 ms) and a weaker fluorescence band around 410 nm (0.5 ns). Similarly, a suspension of **14** exhibited bimodal emission at 450 nm ($\tau_F=0.4$ ns) and 575 nm ($\tau_{RTP}=0.24$ ms). Shown in Figure 4c and 4d are two preliminary examples to demonstrate their application potential. Figure 4c shows that the RTP from a deoxygenated film of **9** slowly decays over a period of 80 ms; this method has great potential for investigating the 3D spatial topology of solid materials over a small area. Figure 4d is an RTP microscopy image of neuronal cells stained by **13** to show that such NNI derivatives are very convenient for biochemical conjugation and could be easily developed as low-cost, time-resolved bioimaging agents.

Table 3: Lifetime and quantum yield data of **6**–**11** under vacuum.

	6	7	8	9	10	11
τ_F[a]	1.75 ns (413 nm)	–[b]	7.0 ns (425 nm)	7.1 ns (450 nm)	7.3 ns (385 nm)	–[b]
τ_{RTP}[a]	5.6 ms (600 nm)	3.6 ms (600 nm)	84 ms (600 nm)	70 ms (600 nm)	–[b]	1.2 s (510 nm)
Φ[c]	0.0020	0.0016	0.027	0.0042	0.068	0.0035
Φ[d]	0.050	0.046	0.0057	0.021	<0.001	0.039

[a] Excitation source: 369 nm light-emitting diode; lifetime fit to triple exponential decay (see the Supporting Information). [b] Emission too weak for reliable lifetime measurements. [c] Absolute photoluminescence quantum yield from 400–500 nm. [d] Absolute photoluminescence quantum yield from 525–750 nm.

Acknowledgements

We acknowledge support from the Fundamental Research Funds for the Central Universities (WK2340000068 and CX2060200022) and the National Natural Science Foundation of China (21222405, 51402282).

Keywords: charge transfer · fluorescence · naphthalimides · organic dyes · phosphorescence

How to cite: *Angew. Chem. Int. Ed.* **2016**, *55*, 9872–9876
Angew. Chem. **2016**, *128*, 10026–10030

[1] J. Li, W. Zhou, X. Ouyang, H. Yu, R. Yang, W. Tan, J. Yuan, *Anal. Chem.* **2011**, *83*, 1356–1362.
[2] G. Zhang, G. M. Palmer, M. Dewhirst, C. L. Fraser, *Nat. Mater.* **2009**, *8*, 747–751.

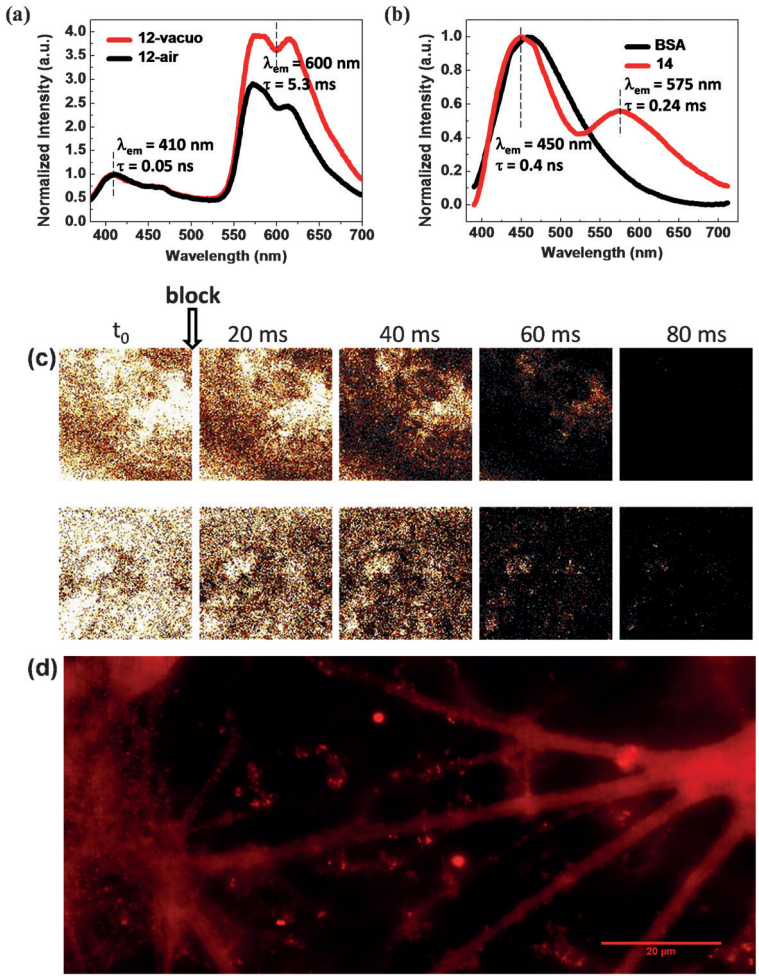

Figure 4. a) Steady-state emission spectra of **12** in air (black) and in vacuo (red) normalized to the fluorescence band. b) Steady-state emission spectra of bovine serum albumin (BSA) aqueous solution (black) and a suspension of **14** in DMSO/H_2O (red) normalized to the fluorescence band (λ_{ex} = 365 nm). c) RTP microscopy of a cast of **9** under vacuum showing images with different time delays. "Block" indicates when a mechanical shutter was closed to block the excitation light (or t_0 for background-free imaging). Imaging area: 0.1 × 0.1 mm^2. d) RTP microscopy of neuronal cells labeled with **13** (10 mg mL^{-1} in DMSO and 50× dilution in PBS buffer; incubation: 10 min). Microscope: Olympus IX71, excitation filter: 330–380 nm, emission filter: 590–650 nm, scale bar: 20 µm.

[3] D. Yu, F. Zhao, C. Han, H. Xu, J. Li, Z. Zhang, Z. Deng, D. Ma, P. Yan, *Adv. Mater.* **2012**, *24*, 509 – 514.

[4] H. Uoyama, K. Goushi, K. Shizu, H. Nomura, C. Adachi, *Nature* **2012**, *492*, 234 – 238.

[5] G. N. Lewis, M. Kasha, *J. Am. Chem. Soc.* **1944**, *66*, 2100 – 2116.

[6] R. C. Evans, P. Douglas, C. J. Winscom, *Coord. Chem. Rev.* **2006**, *250*, 2093 – 2126.

[7] M. Galletta, F. Puntoriero, S. Campagna, C. Chiorboli, M. Quesada, S. Goeb, R. Ziessel, *J. Phys. Chem. A* **2006**, *110*, 4348 – 4358.

[8] A. S. Carretero, A. S. Castillo, A. F. Gutiérrez, *Crit. Rev. Anal. Chem.* **2005**, *35*, 3 – 14.

[9] N. D. McClenaghan, Y. Leydet, B. Maubert, M. T. Indelli, S. Campagna, *Coord. Chem. Rev.* **2005**, *249*, 1336 – 1350.

[10] X. Zhang, T. Xie, M. Cui, L. Yang, X. Sun, J. Jiang, G. Zhang, *ACS Appl. Mater. Interfaces* **2014**, *6*, 2279 – 2284.

[11] P. Lehner, C. Staudinger, S. M. Borisov, I. Klimant, *Nat. Commun.* **2014**, *5*, 1 – 6.

[12] W. Z. Yuan, X. Y. Shen, H. Zhao, J. W. Y. Lam, L. Tang, P. Lu, C. L. Wang, Y. Liu, Z. M. Wang, Q. Zheng, J. Z. Sun, Y. G. Ma, B. Z. Tang, *J. Phys. Chem. C* **2010**, *114*, 6090 – 6099.

[13] Y. Gong, G. Chen, Q. Peng, W. Z. Yuan, Y. Xie, S. Li, Y. Zhang, B. Z. Tang, *Adv. Mater.* **2015**, *27*, 6195 – 6201.

[14] O. Bolton, K. Lee, H. J. Kim, K. Y. Lin, J. Kim, *Nat. Chem.* **2011**, *3*, 205 – 210.

[15] S. K. Maity, S. Bera, A. Paikar, A. Pramanik, D. Haldar, *Chem. Commun.* **2013**, *49*, 9051 – 9053.

[16] Z. An, C. Zheng, Y. Tao, R. Chen, H. Shi, T. Chen, Z. Wang, H. Li, R. Deng, X. Liu, W. Huang, *Nat. Mater.* **2015**, *14*, 685 – 690.

[17] M. H. Lee, J. H. Han, P. S. Kwon, S. Bhuniya, J. Y. Kim, J. L. Sessler, C. Kang, J. S. Kim, *J. Am. Chem. Soc.* **2012**, *134*, 1316 – 1322.

[18] M. H. Lee, J. Y. Kim, J. H. Han, S. Bhuniya, J. L. Sessler, C. Kang, J. S. Kim, *J. Am. Chem. Soc.* **2012**, *134*, 12668 – 12674.

[19] H. Guo, M. L. Muro-Small, S. Ji, J. Zhao, F. N. Castellano, *Inorg. Chem.* **2010**, *49*, 6802 – 6804.

[20] B. Ventura, A. Bertocco, D. Braga, L. Catalano, S. O'Agostino, F. Grepioni, P. Taddei, *J. Phys. Chem. C* **2014**, *118*, 18646 – 18658.

[21] J.-D. Chai, M. Head-Gordon, *Phys. Chem. Chem. Phys.* **2008**, *10*, 6615 – 6620.

[22] J. Tomasi, B. Mennucci, R. Cammi, *Chem. Rev.* **2005**, *105*, 2999 – 3094.

[23] M. W. Schmidt, K. K. Baldridge, J. A. Boatz, S. T. Elbert, M. S. Gordon, J. H. Jensen, S. Koseki, N. Matsunaga, K. A. Nguyen, S. Su, T. L. Windus, M. Dupuis, J. A. Montgomery, *J. Comput. Chem.* **1993**, *14*, 1347 – 1363.

[24] "Advances in electronic structure theory: GAMESS a decade later": M. S. Gordon, M. W. Schmidt, in *Theory and Applications of Computational Chemistry: The First Forty Years* (Eds.: C. E. Dykstra, G. Frenking, K. S. Kim, G. E. Scuseria), Elsevier, Amsterdam, **2005**, pp. 1167 – 1189.

[25] M. J. G. Peach, P. Benfield, T. Helgaker, D. J. Tozer, *J. Chem. Phys.* **2008**, *128*, 044118.

[26] G. Zhang, J. Chen, S. J. Payne, S. E. Kooi, J. N. Demas, C. L. Fraser, *J. Am. Chem. Soc.* **2007**, *129*, 8942 – 8943.

Received: February 3, 2016
Revised: March 29, 2016
Published online: July 7, 2016

